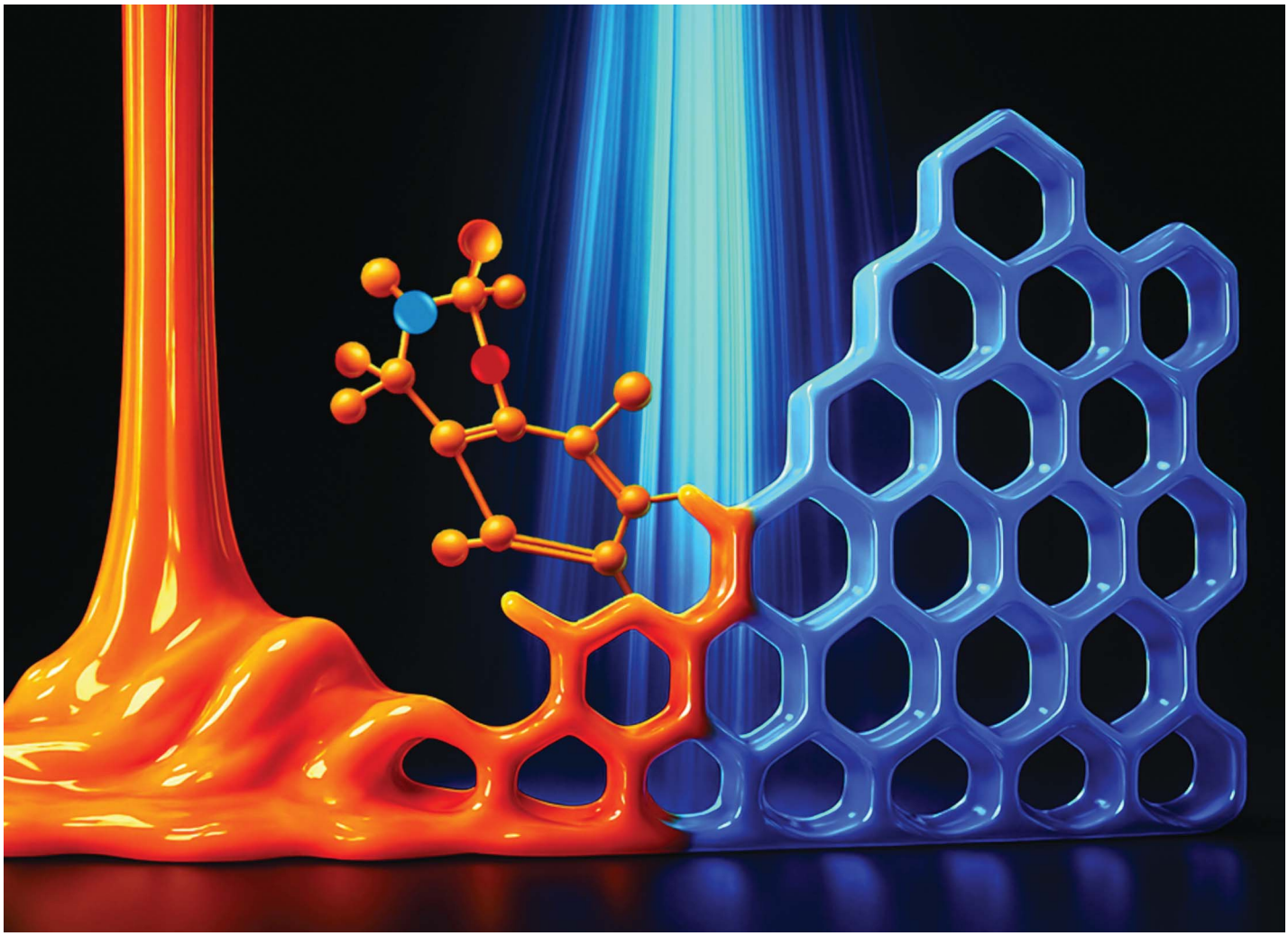

Showcasing a study on UV-curable vitrimers for additive manufacturing applications by a group of researchers led by Dr Pierre Verge from Luxembourg Institute of Science and Technology.

A recyclable, reshapable and UV-curable polybenzoxazine vitrimer enabling closed-loop 3D printing applications

The 3D printing of a bio-based and UV-curable polybenzoxazine vitrimer is demonstrated. Functionalisation of benzoxazine vitrimers with photosensitive methacrylate groups enables material extrusion 3D printing and simultaneous UV curing of the precursors. Thermal post-curing then produces complex parts with interesting thermo-mechanical properties, which can be reshaped and recycled. Ground 3D-printed specimens was used for new prints, closing the recycling loop for this material.

Image reproduced by permission of Pierre Verge from *J. Mater. Chem. A*, 2025, **13**, 34273.

Image generated with Microsoft Copilot.

As featured in:

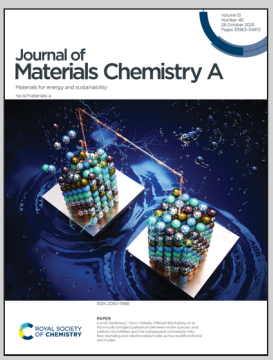

See Pierre Verge *et al.*, *J. Mater. Chem. A*, 2025, **13**, 34273.

ROYAL SOCIETY OF CHEMISTRY

rsc.li/materials-a

Registered charity number: 207890

Journal of Materials Chemistry A

ROYAL SOCIETY OF CHEMISTRY

PAPER

View Article Online
View Journal | View Issue

Cite this: J. Mater. Chem. A, 2025, 13, 34273

A recyclable, reshapable and UV-curable polybenzoxazine vitrimer enabling closed-loop 3D printing applications†

Charles Jehl,[ab] Antoine Adjaoud,[a] Ambre Meyer,[a] Vincent Boulic,[ab] Channya Hesse,[ab] Laura Puchot,[a] Joamin Gonzalez-Gutierrez,[a] Alexander S. Shaplov,[a] Daniel F. Schmidt[a] and Pierre Verge *[a]

The additive manufacturing of a bio-based, UV active, recyclable and reshapable polybenzoxazine is demonstrated. A new ditelechelic benzoxazine monomer (CHDM-PA-mea) was prepared by esterification of phloretic acid (PA) and cyclohexane dimethanol (CHDM)-both chosen for sustainability-and then reacting the product with monoethanolamine (mea) and paraformaldehyde (PFA). This yielded a molecule with two benzoxazine rings, two ester groups and two aliphatic hydroxyls. UV-curability was obtained through partial acylation of the aliphatic hydroxyls to form methacrylates. The modified benzoxazine monomer was then 3D printed *via* UV-assisted materials extrusion, with thermal post-treatment yielding complex parts composed of a fully cured polybenzoxazine vitrimer. The influence of the degree of methacrylation on vitrimer characteristics was explored with the aim of balancing photopolymerisation and printability with vitrimeric properties, as assessed by reshaping and recycling abilities. This work identifies an optimal benzoxazine precursor enabling the production of complex 3D printed vitrimer parts that can be reshaped and recycled, with a T_α of 105 °C, a compressive modulus of 810 MPa and excellent dimensional stability. Ground 3D printed parts were used as viscosity modifiers for new prints, closing the successful recycling loop for this material.

Received 21st February 2025
Accepted 3rd June 2025

DOI: 10.1039/d5ta01478f

rsc.li/materials-a

1 Introduction

Approximately 12% of the global plastic production consists of thermosets.[1] These materials possess high mechanical properties, good thermal stability, and chemical resistance due to their three-dimensional cross-linked structure. As a result, they are widely used in value-added applications, such as aviation and automotive.[2] However, their permanent chemical structure prevents recycling and reshaping. As a result, they are usually landfilled or incinerated once out of service, leading to adverse environmental consequences such as air and soil pollution or the destruction of ecosystems.[3] To address this issue, researchers have developed covalent adaptable networks (CANs), which feature dynamic bonds that can reshuffle under the influence of an external stimulus (temperature, pH, or UV radiation changes), allowing for the structural rearrangement of their network.[4] Vitrimers, a type of associative CAN, have garnered significant interest given their recyclability and reshapability in the absence of depolymerisation.

Among the various families of thermosets modified with dynamic bonds,[5–8] polybenzoxazines provide an efficient combination of high performance and circularity.[9,10] They possess characteristics similar to those of traditional phenolic or epoxy resins such as near-zero shrinkage,[11,12] high glass transition temperatures (T_g> 100 °C),[13,14] high thermal stability (T_{onset}> 200 °C),[15,16] low water absorption,[17] and high mechanical properties.[18–20] The design flexibility and simplicity of the synthesis of benzoxazine monomers allow the use of natural or bio-based precursors[21–27] and the incorporation of dynamic bonds within their structure. Furthermore, the dynamic exchanges can be internally catalysed[9] and accelerated by an efficient mechanism of neighbouring group participation.[28] Finally, benzoxazine vitrimers have been produced based on a wide range of bond exchange reactions: transesterification reactions (TERs) of esters,[29–31] disulfide metathesis,[32–34] boronic ester exchanges,[35] transamination of vinylogous urethanes,[36] imines,[37] siloxane (silyl ethers)[38] and acetal exchanges.[39]

Additive manufacturing has emerged as an attractive area of research due to its promise of design flexibility and waste minimization. Unlike subtractive manufacturing, which entails cutting a material from a block to create an object, additive manufacturing is a computer-controlled process that creates

[a]Luxembourg Institute of Science and Technology (LIST), 5 avenue des Hauts-Fourneaux, Esch-sur-Alzette, L-4362, Luxembourg. E-mail: pierre.verge@list.lu
[b]Department of Physics and Materials Science, University of Luxembourg, 2 Avenue de l'Université, Esch-sur-Alzette, L-4365, Luxembourg

† Electronic supplementary information (ESI) available: See DOI: https://doi.org/10.1039/d5ta01478f

three-dimensional (3D) parts with complex geometries by adding the material layer by layer or section by section[40,41] and finds applications in aerospace, automotive, medicine, electronics, sports equipment, construction and water purification.[42–47] Among the various additive manufacturing techniques, material extrusion additive manufacturing (MEX) has gained significant interest from diverse industries due to its ease of use, cost-effectiveness and low energy consumption since it is possible to perform it at room temperature (RT).[48,49] It also requires only small amounts of resin, making it a clear advantage for demonstrating proof of concept with materials prepared at the lab scale. Finally, MEX 3D printing, which involves depositing a flowable material layer by layer onto a build plate using an extrusion head that can move in three dimensions, is compatible with a broad range of materials, including viscous monomers. In this context, material extrusion proves to be well-suited for very viscous benzoxazine precursors, as opposed to vat photopolymerisation that requires low viscosity precursors. Nevertheless, MEX is highly sensitive to process parameters and monomer properties, which can result in various structural defects in the printed parts (bubbles, geometric deviations, bead width inconsistencies, bumps, voids, shrinkage and poor interlayer adhesion). Consequently, multiple tests are typically required to optimize the design of a part, leading to significant material waste. Thus, the processing of reusable, recyclable vitrimers *via* MEX not only addresses end-of-life concerns but also provides a convenient means of recycling waste generated during process optimization. This synergy represents significant progress with respect to waste reduction and supports the transition to more sustainable production of polymeric products.[50,51]

MEX 3D printing and additive manufacturing in general have not been widely reported in the context of benzoxazines and resultant thermoset materials.[52–54] Similar to the 3D printing of other thermoset resins, the curing process of benzoxazines after printing typically leads to the collapse of the printed structures/parts due to a significant decrease in viscoelastic properties caused by the high temperatures needed for curing.[55] To address this issue, one solution is to develop a benzoxazine-based precursor that can undergo room temperature radical polymerisation during the 3D printing process, allowing the shape of the part to be fixed prior to thermally initiated benzoxazine ring-opening polymerisation (ROP). In this context, a convenient approach is the attachment of (meth)acrylate groups to the benzoxazine-based precursor followed by room-temperature photopolymerisation. Ishida *et al.* were the first to report the methacrylation of the benzoxazine precursor by reacting (3-phenyl-3,4-dihydro-2*H*-benzo[*e*][1,3]oxazin-6-yl)methanol and methacryloyl chloride (mac).[56] Next, Wang *et al.* designed a series of photosensitive benzoxazine oligomers using 2,2′-bis(trifluoromethyl)-4,4′-diaminobiphenyl and 2-isocyanatoethyl methacrylate for the printing of 3D objects by stereolithography.[53] Similarly, Weigand *et al.* developed a UV active benzoxazine compound based on bisphenol-A, 2-(2-aminoethoxy) ethanol and mac for stereolithography.[54]

Inspired by the above-mentioned approach, this work began with the preparation of a new ditelechelic benzoxazine monomer (CHDM-PA-mea) by reacting phloretic acid (PA), which is obtained from the leaves of apple trees,[57] with cyclohexane dimethanol (CHDM), a diol that can be derived from limonene or PET waste.[58,59] This was followed by a reaction with mono-

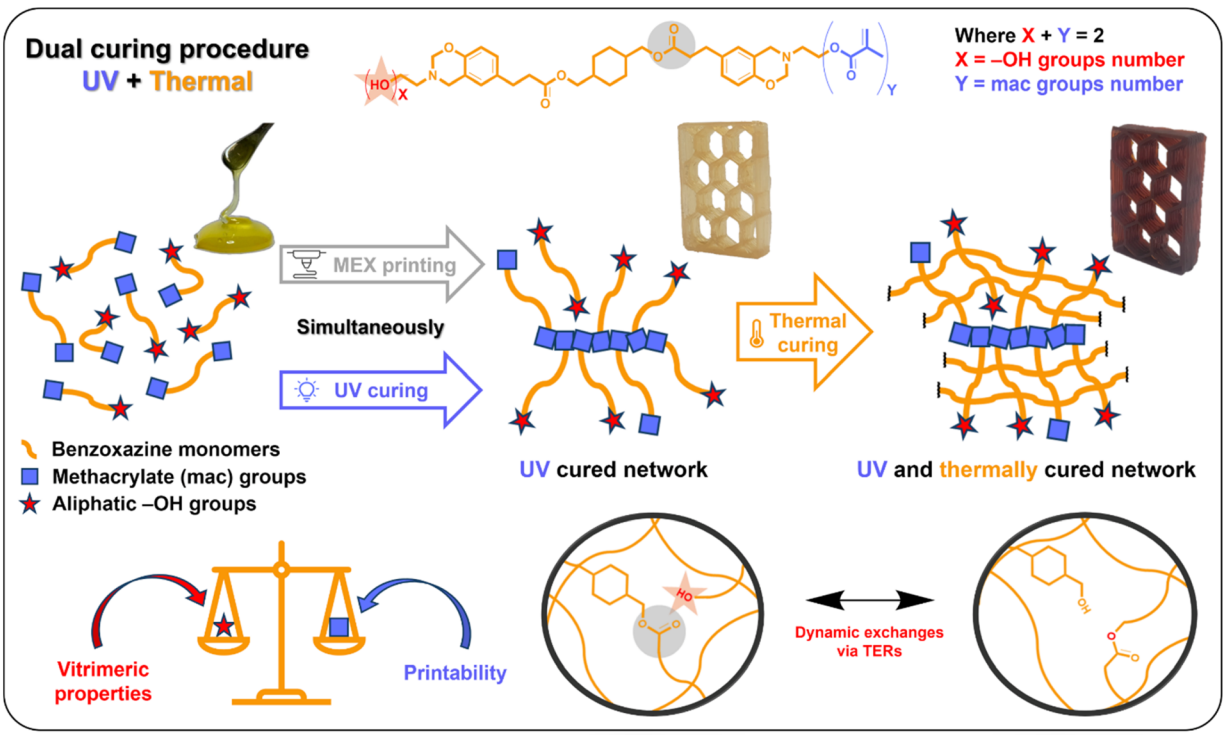

Fig. 1 Strategy suggested for MEX 3D printing of a benzoxazine vitrimer using TERs for dynamic exchanges.

ethanolamine (mea) and paraformaldehyde (PFA), resulting in a molecule composed of two ester groups and containing two aliphatic hydroxyl groups, that can further react by tertiary-amine catalysed TERs following benzoxazine ROP. Sensitivity to photopolymerisation was introduced by partially converting the aliphatic –OH groups into methacrylate groups. It is noteworthy that the methacrylation results in a decrease of the number of –OH groups that are essential for bond exchange in this system.

In this context, the purpose of this study was to develop a dual curing benzoxazine precursor for 3D printing as shown in Fig. 1. In particular, the influence of methacrylation on the characteristics of the vitrimer is explored and the optimal –OH to methacrylate ratio is determined with the goal of balancing photopolymerisability and printability with vitrimeric properties. While the 3D-printed vitrimer parts exhibited excellent reshapability and recyclability, their reuse was successfully demonstrated by grinding them into powder and repeatedly utilizing it as a viscosity modifier for new prints. The finds of these efforts highlight the potential for producing long-lasting thermoset specimens combining additive manufacturing and closed-loop recycling.

2 Experimental section

2.1 Materials

3-(4-Hydroxyphenyl) propionic acid (TCI Europe, > 98.0%, phloretic acid, PA) and 2-aminoethanol (TCI Europe, > 99.0%, monoethanolamine, mea), 1,4-cyclohexanedimethanol (Aldrich, a mixture of cis and trans, 99%, CHDM), *para*-toluene sulfonic acid monohydrate (Aldrich, ≥ 98.5%, *p*-TSA), paraformaldehyde (Aldrich, 95%, PFA), 2,2-dimethoxy-2-phenylacetophenone (Aldrich, 99%, DMPA), fumed silica (Aldrich, amorphous silica powder with an average particle size of 0.2 μm, SiO_2), triethylamine (Carl Roth, ≥ 99.5%, NEt_3), sodium chloride (Carl Roth, ≥99.5%, NaCl), sodium hydroxide (Fisher Scientific, 98%, NaOH) and chloroform (Fisher Scientific, ≥ 99%, $CHCl_3$) were used without purification. Anhydrous dichloromethane (Fisher Scientific, > 99%, DCM) and toluene (Fisher Scientific, > 99%, PhCH3) were obtained from an MBraun SPS-800 solvent purification system. Ultrapure deionized water was obtained using a Sartorius Arium® Comfort Smart Station. Methacryloyl chloride (Aldrich, ≥ 97.0%, mac) was purified by distillation. The distillation was done at atmospheric pressure under a flow of nitrogen while the crude reagent was heated to 110 °C.

2.2 Synthetic procedures

2.2.1 Synthesis of CHDM-PA. The diphenolic terminated CHDM-PA intermediate was synthesized *via* a Fischer esterification. CHDM (17.71 g, 0.123 mol, 1.0 eq.), PA (40.81 g, 0.246 mol, 2.0 eq.) and *p*-TSA (0.09 g, 0.5 wt% based on the diol amount) were reacted solventless in a three-neck round bottom flask at 130 °C for 24 h under mechanical stirring (Ministar 20 Digital, anchor stirrer, 250 rpm) and the flow of argon to remove water and shift the equilibrium reaction toward quantitative ester formation. The dark red paste recovered (53.83 g, 99 wt%) was used without any further purification. According to the ^{1}H NMR spectrum, the purity of the diester was 98% (Fig. S6†)

2.2.2 Synthesis of CHDM-PA-mea. Freshly prepared diphenolic terminated CHDM-PA (46.98 g, 0.107 mol, 1.0 eq.) was reacted solventless with mea (13.07 g, 0.214 mol, 2.0 eq.) and PFA (12.85 g, 0.428 mol, 4.0 eq.) in a three-neck round bottom flask at 85 °C for 2 h 30 min under mechanical stirring (Ministar 20 Digital, anchor stirrer, 250 rpm), undergoing a Mannich-like condensation. The CHDM-PA-mea benzoxazine monomer obtained was dissolved in $CHCl_3$ and dried over magnesium sulfate ($MgSO_4$). The salt was filtered off and the solvent was then evaporated in a rotary evaporator. The precursor was dried overnight under reduced pressure (<1 mBar) at RT, giving an orange honey-like substance (64.74 g, 99 wt%). According to the ^{1}H NMR spectrum, the purity of the benzoxazine monomer was 90% (Fig. S10†).

2.2.3 Synthesis of CHDM-PA-mea/mac. In order to study the impact of the extent of methacrylation on the properties of the final monomer, three critical scenarios were considered: an excess of vitrimer functions, a partial balance of vitrimer and UV-active functions, and an excess of UV-active functions. With this in mind, three different precursors, abbreviated CHDM-PA-mea/mac$_1$-CHDM-PA-mea/mac$_2$-CHDM-PA-mea/mac$_3$, were prepared in the third step using 0.65, 1.35 and 2.05 eq. of mac, respectively. The stoichiometry of the reactants is summarised in Table S1.† The typical synthetic procedure of CHDM-PA-mea/mac$_2$ is given below as an example. The benzoxazine precursor CHDM-PA-mea (19.87 g, 0.033 mol) was loaded into a three-neck round bottom flask, which was then evaporated under high vacuum (<1 mbar) and filled with an argon atmosphere. 100 mL of anhydrous DCM was injected into the flask to form the solution of CHDM-PA-mea under stirring. In the next step, NEt_3 (4.55 g, 0.045 mol) was injected into the flask and stirring was continued at RT until full dissolution. The crude reaction was cooled down to 0 °C in an ice bath and methacryloyl chloride (4.70 g, 0.045 mol) was slowly added dropwise to the reaction medium under magnetic stirring. After the addition of mac, the stirring was continued for 1 h at 0 °C, whereupon the reaction mixture was allowed to warm up to room temperature, and the stirring was continued for an additional 12 h. After completion of the reaction, the triethylammonium salt was filtered off and the solvent was removed using a rotary evaporator. The crude product was dissolved in 300 mL of $CHCl_3$ and purified by liquid–liquid extractions with cold 0.5 M NaOH aqueous solution (3 × 100 mL), cold distilled water (3 × 100 mL), and finally with 20 wt% brine solution (3 × 100 mL). The organic layer was dried over anhydrous magnesium sulfate ($MgSO_4$) and the solvent was evaporated in the rotary evaporator. The resulting CHDM-PA-mea/mac$_2$ precursor was dried overnight under reduced pressure (<1 mBar) at RT to give a yellowish viscous oil (16.45 g, 72 wt%). The conversion of methacryloyl chloride (C) and the acylation degree (AD) of each monomer were determined by ^{1}H NMR using equations S3 and S4 and are summarised in Table S2 (ESI, section 2.21†).

2.2.4 Synthesis of poly$_{UV}$(CHDM-PA-mea/mac) by photopolymerisation of CHDM-PA-mea/mac monomers. The benzoxazine precursor CHDM-PA-mea/mac was mixed with 0.5 per

hundred resins (phr) of DMPA (photoinitiator) and UV cured in an open PTFE mold (6.5 × 1.5 × 0.2 cm) using a UV pen (Hyrel 3D, 365 nm, 5 W). Each face of the specimen was pointed for 10 min using the pen to ensure maximal photopolymerisation. As materials processed in this way are UV-cured only, they are conveniently referred to as poly$_{UV}$(CHDM-PA-mea/mac).

2.2.5 3D printing. The formulations containing CHDM-PA-mea/mac, 0.5 phr of DMPA and either 5.0 phr of fumed silica or 15 phr of recyclate powder (see 2.4.1) were mixed and then degassed under reduced pressure (<1 mBar). The 3D printing trials were performed using the material extrusion (MEX) technique carried out using a Hyrel System 30 M printing device. Materials were extruded at room temperature through a TAM-15 direct ink extrusion head on a glass plate covered with a Teflon film and directly exposed to UV radiation from a Hyrel 3D UV pen (365 nm, 5 W). Printing tests were controlled through the Hyrel Repetrel software with g-codes generated using the Slic3r 1.2.9 software package. Other parameters (nozzle diameter, layer height, and material flow rate multiplier) were adjusted depending on the formulation used (Table S4†).

2.2.6 Thermal curing of CHDM-PA-mea and poly$_{UV}$(CHDM-PA-mea/mac). The CHDM-PA-mea monomers and poly$_{UV}$(-CHDM-PA-mea/mac) materials were thermally cured to form poly(CHDM-PA-mea) and poly$_{UV+\Delta T}$(CHDM-PA-mea/mac), respectively. Thermal curing was performed at 170 °C for 1 h in air using a forced convection oven (Binder M–53).

2.3 Characterisation methods

2.3.1 Rheological monitoring of UV curing. Rheological analysis was performed on a Physica MCR 302 (Anton Paar) rheometer equipped with a CTD 450 temperature control device. The UV curing was monitored by coupling the rheometer with an Excelitas Omnicure S1500 UV curing system generating UV radiation from 250 to 450 nm with a power of 200 W. The UV polymerisation of CHDM-PA-mea/mac precursors was performed by loading samples with 0.5 phr of DMPA as a photoinitiator between an aluminium plate and a glass plate allowing the light from the UV curing device to pass through (diameter = 25 mm, gap = 0.25 mm). Measurements were performed at room temperature in the oscillation mode with an amplitude of 0.1% and a frequency of 10 Hz. UV exposure was started 50 s after the beginning of the analysis.

2.3.2 Stress relaxation measurements. Stress relaxation tests were conducted in torsion mode using a geometry composed of two parallel fixing clamps. A constant strain of 1% was applied to bar-shaped samples of 25 × 5 × 1.5 mm clamped at both ends. The relaxation modulus was followed as a function of time until 6000 s at 140, 150, 160 and 170 °C. The relaxation time (τ^*) was set as the time required for the material to reach 1/e (0.37) of its original modulus.[4] Activation energies (E_a) were determined using the slope of the Arrhenius plot according to eqn (1):

$$\ln(\tau^*) = \frac{E_a}{RT} - \ln(A) \quad (1)$$

2.3.3 X-ray micro-computed tomography (μCT). μCT analyses were conducted with an X-ray cone beam machine EasyTom 160 from RX Solutions. X-rays were generated with a micro-focused tube (tungsten filament, small focus spot mode). The detector used was a 16-bit flat panel imager with a total pixel area of 1920 pixels × 1536 pixels. The 3D reconstruction of the sample volume into stacked slices has been conducted with the Xact64 (RX Solutions) software after applying a sample movement correction (spot deviation module) and a system misalignment correction (geometry correction module). The analysis of the stacked slices was conducted by means of the Avizo (Konrad-Zuse-Zentrum Berlin/FEI SAS-Thermo Fisher Scientific) software.

2.3.4 Compression tests. Compression testing was performed on 3D printed honeycombs using an INSTRON 5967 electromechanical testing machine. Samples were placed between two aluminium plates, with the upper plate set to move at a fixed speed of 0.5 mm min^{-1}. Tests were conducted until the specimen was broken. The compressive stress for each specimen was calculated using the compressive force applied and the average surface area of all sample layers as determined by μCT. The compressive modulus was estimated from the slope of the compressive stress–strain curve.

Other characterisation techniques are reported in the ESI.†

2.4 Recycling

2.4.1 Mechanical grinding. For sample reprocessing, materials were ground at room temperature with a laboratory blender from M.R.C. (Rachmanov Bukshtein) LTD operating at 22 000 rpm for 40 s. To prepare materials for reuse in 3D printing, specimens were first cooled with liquid nitrogen and then ground into a fine powder with a Retsch ZM 200 centrifugal mill using an 80 μm sieve at 18 000 rpm for 20 s.

2.4.2 Chemical degradation. Materials were degraded by immersion in an aqueous formic acid solution (25 mg/2 mL) maintained at 80 °C. A powder was recovered after evaporation of the acidic solution *via* rotary evaporation. The powder was then dried at 50 °C for 12 h and further at 100 °C for 2 h under reduced pressure (<1 mbar).

2.4.3 Reprocessing. The resulting powders (produced either mechanically or chemically) were placed into a disk-shaped mold (30 mm or 8 mm in diameter). The mold was preheated at 170 °C for 3 min and then pressed under 28 MPa of pressure at 170 °C for 30 min between the heated platens of a Carver 12 ton hydraulic laboratory press (Model 3851-0). Afterwards, the mold was removed from the press, and the reprocessed samples were taken out of the mold and cooled to room temperature.

Reprocessing was also done *via* MEX; here, ground powder was added to fresh resin and the MEX process was repeated, as described in 2.2.5.

3 Results and discussion

3.1 Structural characterisation of monomers

The synthesis of benzoxazine monomers with methacrylic functional groups is illustrated in Fig. 2a. The structure and

purity of all products were estimated *via* NMR and FTIR analyses (Fig. S6–S8, S10–S12 and S15–S20†). During Fischer esterification, the clear disappearance of the peaks associated with the aliphatic hydroxyl groups of CHDM (δ = 3.15–3.30 ppm, CH_2*–OH [$2_{trans/cis}$], Fig. S1†) in the ^{1}H spectrum of CHDM-PA (Fig. S6†) highlights the almost quantitative conversion of the diol to the desired diester despite the existence of two CHDM isomers. This process was accompanied by the appearance of a strong band at 1702 cm^{-1} attributed to the C=O vibration of the newly formed esters, several bands at 1480–1510 cm^{-1} assigned to the C=C stretching vibrations of the aromatic rings, a band at 825 cm^{-1} designated to out-of-plane C–H vibration in the *para*-substituted aromatic ring, and a shift of the broad band at ~3300 to ~3400 cm^{-1} associated with the substitution of aliphatic O–H stretches to the aromatic ones (Fig. S8†).

After the Mannich-like condensation reaction, the ^{1}H NMR spectrum of the CHDM-PA-mea product (Fig. S10†) reveals the characteristic peaks of the benzoxazine rings, at δ = 3.91 and δ = 4.77 ppm, corresponding to N–CH_2*–Ar [5] and N–CH_2*–O [4], respectively. The peaks at δ = 6.65 ppm and δ = 6.99 ppm are attributed to the phenolic protons of CHDM-PA, indicating the presence of some residual reactant. The experimental integration of the methylene protons of the N–CH_2*–O signal counted for 2.88H (4.00H theoretical), indicating that 72% of the oxazine rings were closed. As reported in other work, the remaining 28% consists of the starting ester (10%) and an oxazolidine substructure (18%) (Fig. S9, [a–f] in S10†).[28]

In the IR spectrum of the CHDM-PA-mea product in comparison with the CHDM-PA precursor, the decrease in the intensity of the O–H stretching vibrations at 3446 cm^{-1}, the shift of the characteristic C=O band from 1702 to 1728 cm^{-1}, the increase in the aliphatic C–H stretching at 2720–3060 cm^{-1} and the

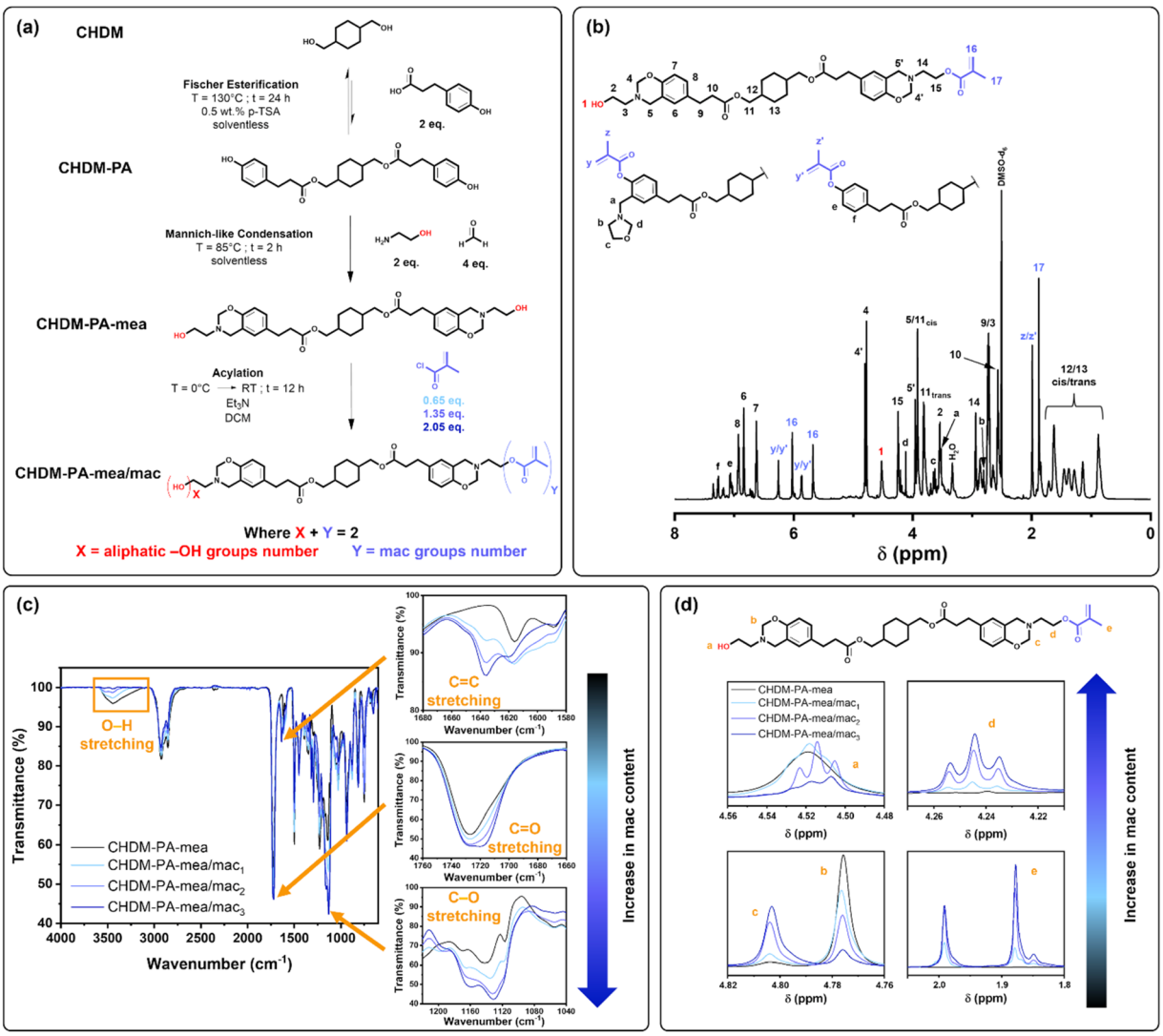

Fig. 2 (a) Synthetic route for photopolymerisable benzoxazine precursors; (b) ^{1}H NMR spectrum of the main structure of CHDM-PA-mea/mac_2 precursor and related substructures; (c) FTIR spectra of CHDM-PA-mea and CHDM-PA-mea/mac precursors highlighting characteristic peaks (simplified spectra; see full spectra in Fig. S20†); (d) focus on regions of ^{1}H NMR spectra of CHDM-PA-mea and CHDM-PA-mea/mac precursors (simplified spectra; see full spectra in Fig. S18†).

appearance of several bands at 1228 and 968–696 cm^{-1} attributed to the C–O–C vibration of the oxazine ring and C–H stretching of the tri-substituted aromatic rings were observed (Fig. S12†).

Regarding the third step of the synthesis, it was concluded from ^{1}H NMR spectra of the monomers (Fig. S15 and S18†) that the experimental conditions used for the methacrylation favoured the formation of oxazolidine substructures. Indeed, the experimental integrations of N–CH_2*–O [4, 4′] decrease from 2.88 to 2.10 between the starting benzoxazine and the benzoxazine produced using large amounts of mac and NEt_3 (Fig. S18†). Furthermore, the presence of several peaks in the ranges of δ = 5.60–6.30 ppm and δ = 1.85–2.00 ppm, corresponding to CH_2* = C(CH_3)–CO [16, *y*, *y*′] and CH_2 = C(CH_3*)–CO [17, *z*, *z*′] (Fig. 2b and S15†), respectively, tends to indicate that methacrylate groups were grafted on different sites. The signals corresponding to the oxazolidine structure and the starting ester are all shifted between the ^{1}H NMR spectrum of CHDM-PA-mea ([a–f], Fig. S10†) and the ^{1}H NMR spectrum of CHDM-PA-mea/mac_2 ([a–f], Fig. 2b and S15†), indicating a change in their chemical environment. This implies that mac reacted both with the aliphatic hydroxyl groups from mea counterparts and the phenolic hydroxyl groups coming either from oxazolidines or from unreacted CHDM-PA. Furthermore, the ^{1}H NMR and FTIR analyses of CHDM-PA-mea/mac monomers demonstrated the impact of mac concentration on the chemical modification and acylation degree (AD of 31, 60 and 94% for CHDM-PA-mea/mac_1, CHDM-PA-mea/mac_2 and CHDM-PA-mea/mac_3, respectively, Table S2†). Specifically, the bands at 3446 and 1030 cm^{-1} attributed to the –OH vibrations progressively disappeared, while the intensity of the bands at 1735 (C=O) and 1635 (aliphatic C=C) cm^{-1} associated with the formation of methacrylate groups increased with the increase of the amount of mac (Fig. 2c). The same trend can be observed in the NMR spectra as well (Fig. 2d).

3.2 Thermal behaviour of precursors

The differential scanning calorimetry (DSC) curves of all monomers are presented in Fig. 3a. The first exothermic peak ($T_{exo,1}$ = 105–223 °C) is observed for CHDM-PA-mea corresponding to the ring opening of the benzoxazine rings. This peak is in the same range as the one observed in benzoxazine vitrimers with a similar structure.[29–31] The second exothermic peak centred around 250 °C ($T_{exo,2}$) is attributed to thermal degradation, as confirmed by thermogravimetric analysis (TGA, Fig. S21†). The presence of exothermic peaks for CHDM-PA-mea/mac_1 and CHDM-PA-mea/mac_2 in the range of 125–228 °C shows that the ring opening of benzoxazine still occurs, even in the presence of methacrylate groups. However, their T_{onset} values are shifted to higher temperatures compared to CHDM-PA-mea. This may be explained by the fact that these monomers contain fewer aliphatic hydroxyl groups, which are known to catalyse the ring opening of benzoxazine.[60–62] The exothermic peak attributed to the ring opening reaction of CHDM-PA-mea/mac_3 is slightly shifted towards higher temperatures, but a new, lower temperature exotherm ($T_{exo,0}$ = 102–164 °C) is also observed. This is attributed to the thermally induced polymerisation of the highly reactive methacrylate functions prior to benzoxazine ring opening.

The precursors were also subjected to rheokinetic measurements, with results shown in Fig. 3b. The data present the evolution of the complex viscosity of each monomer with increasing temperature. The curves show that the CHDM-PA-mea/mac systems display similar curing behaviour to the CHDM-PA-mea precursors upon heating. Gelation occurs more slowly as the extent of methacrylation increases, underlining the impact of –OH functions on the ROP of benzoxazines. However, the rapid increase in the complex viscosity of CHDM-PA-mea/mac_3 at around 828 s is likely due to the polymerisation of the methacrylate functions, which form a preliminary acrylate network, confirming the conclusion drawn from DSC measurements.

3.3 Photopolymerisation of functionalized monomers

The UV curability of the precursors was investigated following the addition of DMPA as a radical initiator (0.5 phr) by performing rheokinetic measurements at room temperature under UV exposure. The graph shows the evolution of the complex

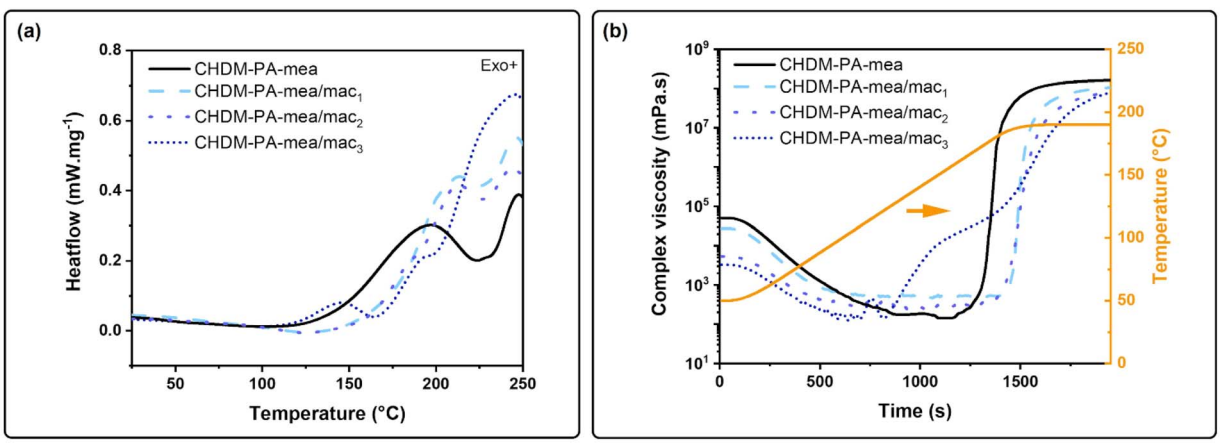

Fig. 3 (a) DSC curves and (b) rheokinetic measurements of CHDM-PA-mea and CHDM-PA-mea/mac monomers.

viscosity of each resin as a function of time when exposed to UV irradiation (Fig. 4a).

A significantly lower initial viscosity is observed in the functionalized resins compared to CHDM-PA-mea. This reduction can be attributed to the introduction of methacrylate functions, which decrease the number of hydroxyl groups and, consequently, the number of intermolecular hydrogen bonding interactions. Then, the curves show that the complex viscosity of each mac-functionalized monomer increases once UV irradiation starts. The curves showing the evolution of storage and loss moduli were used to determine the gelation time (Fig. S22†). As expected, it decreases with the amount of acrylate functionalities, from 84 to 16 to 4 s for CHDM-PA-mea/mac$_1$ to CHDM-PA-mea/mac$_3$.

Poly$_{UV}$(CHDM-PA-mea/mac), referring to specimens that have only been UV cured, were subjected to dynamic mechanical thermal analyses to assess their α-transition temperature (T_α) as illustrated in Fig. 4b. T_α increases with the amount of mac, ranging from 19 °C for poly$_{UV}$(CHDM-PA-mea/mac$_1$) to 70 °C for poly$_{UV}$(CHDM-PA-mea/mac$_3$), showing that with more methacrylate functions, a higher cross-linking density is reached for poly$_{UV}$(CHDM-PA-mea/mac) systems. Thus, a better shape retention can be expected when they are exposed to heat. The curves of the storage modulus confirm these observations, showing an increase in the rubbery plateau with increasing mac content (Fig. S23†).

The evolution of cross-linking density was also checked by swelling experiments of poly$_{UV}$(CHDM-PA-mea/mac) in water and toluene (Fig. S24†). In water, swelling ratios are 7.1%, 3.1% and 1.8% for poly$_{UV}$(CHDM-PA-mea/mac$_1$), poly$_{UV}$(CHDM-PA-mea/mac$_2$) and poly$_{UV}$(CHDM-PA-mea/mac$_3$) respectively. In toluene, poly$_{UV}$(CHDM-PA-mea/mac$_3$) remained cohesive after more than 800 h of immersion, while poly$_{UV}$(CHDM-PA-mea/mac$_2$) broke into small pieces after 170 h and poly$_{UV}$(CHDM-PA-mea/mac$_1$) after only 3 h.

Insets of Fig. 4b capture the ability of 2 mm thick bar of each poly$_{UV}$(CHDM-PA-mea/mac) to resist bending when a 50 g weight is applied to its extremity, illustrating an increase in the modulus with the mac content.

3.4 Characterisation of dual-cured materials

DSC measurements were performed on poly$_{UV}$(CHDM-PA-mea/mac). As expected, the first exothermic peak observed in the thermogram of CHDM-PA-mea/mac$_3$ and associated with methacrylate polymerisation is not visible anymore (Fig. 5a). Interestingly, the exothermic peak ($T_{exo,1}$) centred around 215 °C indicates that the opening of the benzoxazine rings still occurs after the reaction of the methacrylate functions.

Dynamic TGA analyses of poly$_{UV}$(CHDM-PA-mea/mac) materials have been carried out and show that no degradation occurs until 230 °C (Table 1, column 3, Fig. S25†). In addition, static TGA analyses of these specimens reveal a mass loss of 4.2%, 2.5% and 3.9% for poly$_{UV}$(CHDM-PA-mea/mac$_1$), poly$_{UV}$(CHDM-PA-mea/mac$_2$) and poly$_{UV}$(CHDM-PA-mea/mac$_3$), respectively, after 3 h at 170 °C (Fig. S26†). As the observed values are all significantly lower than what would be expected in the case of loss of the methacrylate groups (~6 wt%, ~12 wt% and ~17 wt%), this can be attributed to the departure of volatiles such as moisture rather than thermal degradation, providing evidence for stability upon thermal curing.

Dual-cured poly$_{UV+\Delta T}$(CHDM-PA-mea/mac) systems were then obtained after a thermal treatment of single cured poly$_{UV}$(CHDM-PA-mea/mac) samples at 170 °C for 1 h. DSC data, reported in Fig. S27,† show that the treatment is enough to fully open the benzoxazine rings.

TGA measurements were also performed to assess the thermal stability of each dual-cured polymer (Fig. S28†). The results indicate that the stability increases with the introduction of mac, with a 5% weight loss reached at 236 °C for poly(CHDM-PA-mea) and around 270 °C for poly$_{UV+\Delta T}$(CHDM-PA-mea/mac) materials (Table 1, column 7). Presumably, the substitution of dangling hydroxyl groups by polymerised methacrylate functions enhances the thermal stability of the resulting network.

Dynamic mechanical thermal analyses were also performed on dual-cured systems. The additional thermal treatment leads to a significant increase in T_α, for instance, from 43 to 105 °C in the case of poly$_{UV+\Delta T}$(CHDM-PA-mea/mac$_2$) as depicted in Fig. 5b, as a consequence of higher cross-linking density

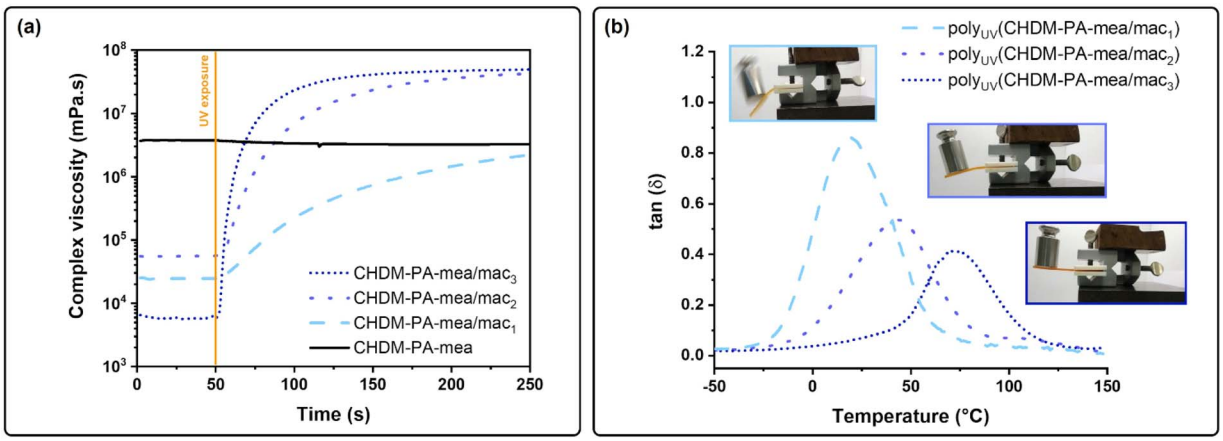

Fig. 4 (a) Isothermal UV rheokinetic measurements of CHDM-PA-mea/mac monomers at room temperature; (b) rheology temperature sweep curves in torsion mode of poly$_{UV}$(CHDM-PA-mea/mac) materials and photos of sample bending (room temperature).

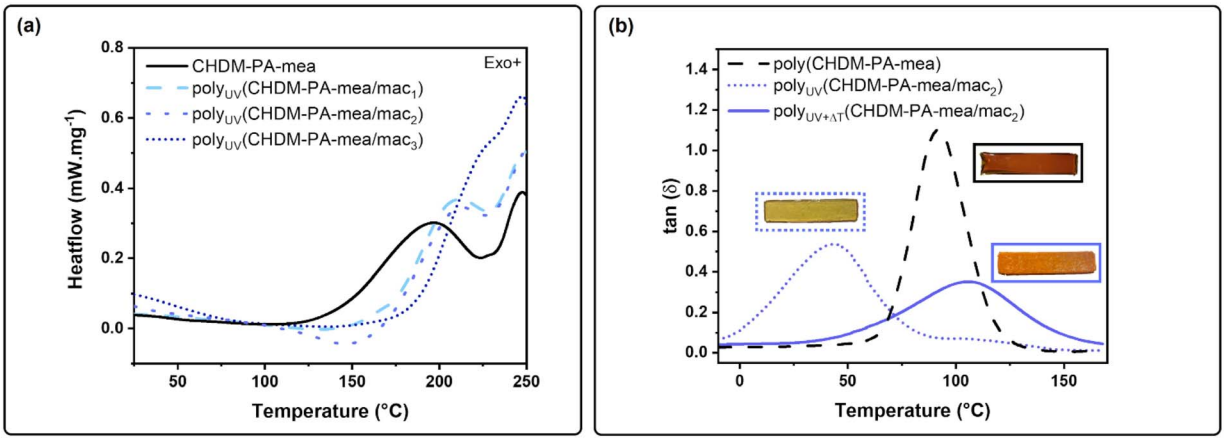

Fig. 5 (a) DSC curves of the CHDM-PA-mea precursor and poly$_{UV}$(CHDM-PA-mea/mac); (b) rheology temperature sweep curves in torsion mode of poly(CHDM-PA-mea), poly$_{UV}$(CHDM-PA-mea/mac$_2$) and poly$_{UV+\Delta T}$(CHDM-PA-mea/mac$_2$) with photos of samples tested.

resulting from the ROP of benzoxazines (Fig. S29†). The same trend is observed for the other compositions (Table 1, columns 2 and 6). Moreover, the completion of the thermal curing results in an increase of the rubbery plateau of poly$_{UV+\Delta T}$(CHDM-PA-mea/mac) materials compared with their single UV cured counterparts (Fig. S30†). Interestingly, the rubbery plateau modulus of dual-cured samples also increases with the extent of methacrylation, which suggests that the methacrylates are not degraded during thermal curing.

The evolution of the cross-linking density, monitored by swelling experiments of poly$_{UV+\Delta T}$(CHDM-PA-mea/mac) in water and toluene (Fig. S31†), is also explained by this behaviour. Unlike single cured materials, dually cured samples no longer swell in toluene as a result of the ROP of benzoxazine (Table 1, columns 4 and 8). In water, thermally cured samples all have a similar swelling ratio, independent of mac content and slightly higher than that of the poly(CHDM-PA-mea) reference. This may be explained by a balance between increased crosslink density and the polarity variations arising from the changes in the content of polymerised methacrylate groups and phenolic rings. Interestingly, the crosslink density increases without a corresponding increase in T_g, which can be explained by that the methacrylate crosslinks are more flexible than benzoxazine crosslinks, indicating partial retention of the methacrylates.

3.5 Vitrimeric behaviour

TERs govern the vitrimeric behaviour of poly(CHDM-PA-mea) and poly$_{UV+\Delta T}$(CHDM-PA-mea/mac). The TER is a mechanism that requires both ester bonds and –OH groups, usually in the presence of a catalyst that promotes faster dynamic exchange. In the case of benzoxazine-based vitrimers relying on the TER, tertiary amines generated from benzoxazine ROP play the catalytic role,[28,63] but the excess of available aliphatic –OH over ester bonds groups also plays a major role.[30,64]

As a result, it can be foreseen that methacrylation, which substitutes aliphatic –OH groups, will impact the efficiency of the dynamic process and impede the vitrimeric behaviour. The effect of methacrylation was assessed by stress relaxation measurements at different temperatures (Fig. S32†). The relaxation time (τ^*), which corresponds to the time needed for a material to reach 1/e (0.37) of its original modulus,[4] is a good representation of the ability of the material to behave as a vitrimer. It was determined for each polymer and plotted in Fig. 6a as a function of the temperature. Clearly, the relaxation time becomes significantly longer with increasing mac content as a result of the decreased number of –OH groups involved in TERs. The activation energies (E_a) of poly$_{UV+\Delta T}$(CHDM-PA-mea/mac) systems were determined and are all in the same range (Fig. S33†).

Table 1 Summary of the thermal and swelling properties of poly$_{UV}$(CHDM-PA-mea/mac), poly(CHDM-PA-mea) and poly$_{UV+\Delta T}$(CHDM-PA-mea/mac) materials

	UV cured				UV + thermal cured			
Network	T_α[a] [°C]	$T_{5\%}$[b] [°C]	$W_{toluene}$ [%]	W_{water}[e] [%]	T_α [°C]	$T_{5\%}$ [°C]	$W_{toluene}$[e] [%]	W_{water}[e] [%]
CHDM-PA-mea	—	—	—	—	92	236	0.1 ± 0.0	1.7 ± 0.1
CHDM-PA-mea/mac$_1$	19	231	8.3 ± 1.1[c]	7.1 ± 0.1	85	275	0.4 ± 0.4	2.7 ± 0.5
CHDM-PA-mea/mac$_2$	43	266	9.8 ± 0.2[d]	3.1 ± 0.1	105	275	0.4 ± 0.4	2.6 ± 0.0
CHDM-PA-mea/mac$_3$	70	253	1.3 ± 0.2[e]	1.8 ± 0.3	124	278	0.5 ± 0.3	2.3 ± 0.4

[a] Determined from the maximum of the tan δ curve in rheology temperature sweep measurement in torsion mode. [b] Temperature of 5% of weight loss determined by TGA. [c] Determined just before breaking after 3 hours of immersion in toluene. [d] Determined just before breaking after 170 hours of immersion in toluene. [e] Determined after 200 hours of immersion in solvent.

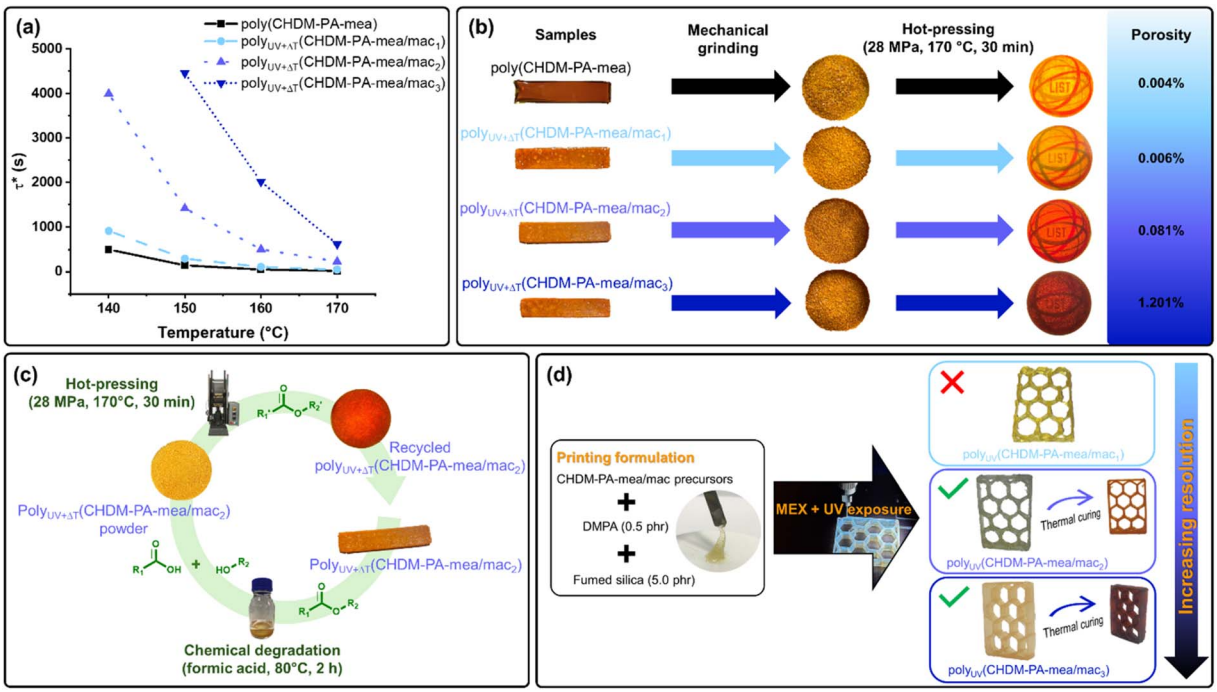

Fig. 6 (a) Evolution of relaxation times of each poly$_{UV+\Delta T}$(CHDM-PA-mea/mac) composition as a function of temperature; (b) photographs of the mechanical recycling of poly$_{UV+\Delta T}$(CHDM-PA-mea/mac); (c) chemical recycling strategy adopted for poly$_{UV+\Delta T}$(CHDM-PA-mea/mac$_2$); (d) photographs of honeycombs obtained after 3D printing trials by MEX with CHDM-PA-mea/mac precursor based formulations.

Both chemical and mechanical recycling were performed on dual-cured materials as illustrated in Fig. 6b and c, respectively. Micro-computed tomography (μCT) analyses performed on mechanically recycled discs revealed that the internal porosity increases with the rate of mac functionalization, from 0.006% and 0.081% to 1.201% for poly$_{UV+\Delta T}$(CHDM-PA-mea/mac$_1$), poly$_{UV+\Delta T}$(CHDM-PA-mea/mac$_2$) and poly$_{UV+\Delta T}$(CHDM-PA-mea/mac$_3$), respectively, illustrating in all cases a good reconsolidation of the material even if for poly$_{UV+\Delta T}$(CHDM-PA-mea/mac$_3$) the level of porosity could be of concern (Fig. S34†). Poly$_{UV+\Delta T}$(CHDM-PA-mea/mac$_2$) was reprocessed in a similar way after targeted chemical degradation in formic acid. This first step is presumed to involve acid hydrolysis of the esters, resulting in the formation of the corresponding carboxylic acids and alcohols (Fig. S35†). In this scheme, the hot-pressing of the degraded material facilitates reformation of the esters. μCT analyses showed evidence of effective reconsolidation of the recovered material (<2% internal porosity). Dynamic mechanical thermal experiments and swelling tests were conducted to assess the effect of recycling on the properties of the reprocessed materials with various mac contents. Recycling processes—both mechanical and chemical—were found to increase the T_α of the materials, indicating altered mobility of the polymer segments (Table 2, column 3, Table S3 and Fig. S36 and S37†). Notably, this shift occurred without significant changes in the rubbery modulus or swelling behaviour (Table 2, columns 5–7), suggesting that the crosslinking density remains largely unaffected. In the case of poly$_{UV+\Delta T}$(CHDM-PA-mea/

Table 2 Summary of the thermo-mechanical and swelling properties of pristine and reprocessed poly$_{UV+\Delta T}$(CHDM-PA-mea/mac) materials

Network		T_α[c] [°C]	T_g[d] [°C]	G'[e] [GPa]	W_{water} [%]	$W_{toluene}$ [%]
poly$_{UV+\Delta T}$(CHDM-PA-mea/mac$_1$)	Pristine	85	59	0.02	2.7 ± 0.5[f]	0.4 ± 0.4[f]
	MR[a]	103	75	0.02	1.1 ± 0.1[g]	0.1 ± 0.0[g]
poly$_{UV+\Delta T}$(CHDM-PA-mea/mac$_2$)	Pristine	105	64	0.03	2.6 ± 0.0[f]	0.4 ± 0.4[f]
	MR	116	76	0.04	1.0 ± 0.1[g]	0.0 ± 0.5[g]
	CR[b]	126	84	0.02	4.9 ± 0.2[g]	0.0 ± 0.0[g]
poly$_{UV+\Delta T}$(CHDM-PA-mea/mac$_3$)	Pristine	124	83	0.08	2.3 ± 0.4[f]	0.5 ± 0.3[f]
	MR	137	88	0.09	1.3 ± 0.3[g]	0.0 ± 0.1[g]

[a] Mechanical recycling. [b] Chemical recycling. [c] Determined from the maximum of the tan δ curve in rheology temperature sweep measurement in torsion mode. [d] Determined from the maximum of the loss modulus curve in rheology temperature sweep measurement in torsion mode. [e] Determined within the rubbery plateau region (T_α + 40 °C) in rheology temperature sweep measurement in torsion mode. [f] Determined after 200 hours of immersion in solvent. [g] Determined after 150 hours of immersion in solvent.

mac_2), T_α increased from 105 °C to 116 °C after mechanical recycling and up to 126 °C after chemical recycling, likely due to degradation of the polymethacrylate segments. These findings demonstrate that recycled materials retain comparable network integrity while exhibiting changes in chain mobility, highlighting the effectiveness of the recycling approaches.

In summary, dual cured materials are recyclable by hot pressing. However, the rate of methacrylation influences the vitrimeric behaviour of the final material. This is illustrated by the short relaxation times and good recyclability of $poly_{UV+\Delta T}$(CHDM-PA-mea/mac_1) and $poly_{UV+\Delta T}$(CHDM-PA-mea/mac_2). $Poly_{UV+\Delta T}$(-CHDM-PA-mea/mac_3) has more limited reshaping and recycling properties due to the lower amount of aliphatic –OH groups able to react through dynamic TERs and the higher crosslink density generated by permanent polymethacrylate parts.

3.6 3D printing of benzoxazine monomers

CHDM-PA-mea/mac monomers were 3D printed by MEX to achieve honeycomb-like structures as shown in Fig. 6d. For this aim, the fluid material is applied to a flat surface using an extrusion head that can move in a Cartesian plane to build the structure layer by layer, while being simultaneously exposed to UV irradiation. This triggers the photopolymerisation of the methacrylate groups, providing mechanical support to the printed material to withstand thermal exposure during the benzoxazine crosslinking step. Each precursor was printed using this method to form a hexagonal honeycomb. Due to the low viscosity of the precursor, 5 phr of fumed silica was added as a viscosity modifier to the printing formulations containing the resin and the radical initiator (DMPA, 0.5 phr). The impact of silica on resin viscosity was assessed by viscosity measurements (Fig. S38†). The printing parameters used to build honeycombs with these resins are summarised in Table S4.†

According to the UV isothermal rheokinetic measurements, shorter gelation times are achieved with higher mac content. In practice, it is illustrated by the better definition and resolution of the honeycomb structures, both before and after thermal curing. For CHDM-PA-mea/mac_1, the methacrylate content is too low to achieve a well-defined structure. Moreover, in this configuration only, the printing formulation tends to stick to the nozzle, leading to heterogeneities during the deposition process and defects in the printed part. A minimum amount of UV-active functionality is therefore required to ensure fast gelation and acceptable dimensional stability. CHDM-PA-mea/mac_2 and CHDM-PA-mea/mac_3 are suitable for this type of application. Printed parts were thermally cured for 1 h at 170 °C to complete the ROP of benzoxazines, validating the approach.

3.7 Properties of 3D printed parts

Among the formulations, only CHDM-PA-mea/mac_2 and CHDM-PA-mea/mac_3 enable 3D printing with good resolution (Fig. 6d). In addition, CHDM-PA-mea/mac_2 offers the most significant vitrimeric properties (Fig. 6a–c). Therefore, it was selected for printing a demonstrator to undergo testing.

μCT analyses were performed to determine the effective volume of a printed honeycomb before and after the completion of thermal curing (Fig. 7a). The results revealed a volumetric shrinkage of 6%, comparable to other low shrinkage resins used for 3D printing applications.[53,65] It is important to note that the shrinkage observed does not result from the curing process—known to be minimal in benzoxazines—but rather from chain orientation and stress relaxation phenomena occurring during the extrusion and deposition phases of the 3D printing process. No delamination or defects between the layers were observed by optical microscopy, attesting to the good adhesion of the material layers during deposition and the dimensional stability of the printed part during the thermal treatment (Fig. 7b).

3.8 Reshaping, mechanical and chemical recycling of 3D printed parts

The benefit of having dynamic bonds within the network was revealed through reshaping, welding and both mechanical and chemical recycling of printed honeycombs. Fig. 7c illustrates that the printed and dual-cured honeycomb can be deformed without fracture at 170 °C over 5 min, demonstrating the ease of reshaping of such 3D printed structures. Fig. 7d shows the successful welding of two halves of a honeycomb into a single self-supported piece after maintaining both parts in contact for 30 min at 170 °C.

Mechanical recycling was assessed by grinding 3D printed parts and then successfully reconsolidating them *via* hot pressing. 3D printed parts were also degraded under acidic conditions at 80 °C. After drying to remove the reaction media, a powder was recovered and reprocessed under conditions identical to those used for mechanical recycling, leading to fully self-supported materials. Recycled samples are all well reconsolidated, with internal porosities of 2.33% and 3.65% for the mechanically and chemically recycled specimens, respectively (Fig. 7e).

The potential to close the recycling loop was demonstrated by reusing powder obtained from grinding printed honeycomb structures as a viscosity modifier in new printing tests. As shown in Fig. 7f, 15 phr of mechanically ground powder was added to fresh resin containing 0.5 phr of a radical initiator to adjust the viscosity of the formulation (Fig. S38†), enabling the printing of new honeycombs. Compression testing of the initially printed honeycombs (Fig. 7g) revealed a compressive modulus of 810 MPa and a strength at break of 80 MPa, comparable to other polymeric 3D-printed honeycombs.[66–69] The sample printed with recycled powder achieved a compressive modulus of 690 MPa and an ultimate strength of 120 MPa, demonstrating the feasibility of producing high-performance parts using this recycling strategy. μCT imaging of the printed bead revealed no porosity, indicating strong interactions between recycled material grains and the matrix that likely contributed to the retention of mechanical properties. The lower compressive modulus and increased strength at break for the recycled powder-based part can be explained by the reduction in silica content, which made the initial honeycomb more rigid and brittle.[70] For context, Nomex-resin honeycombs—commonly used in structural applications—exhibit compressive moduli around 1.5 GPa due to the reinforcement provided by

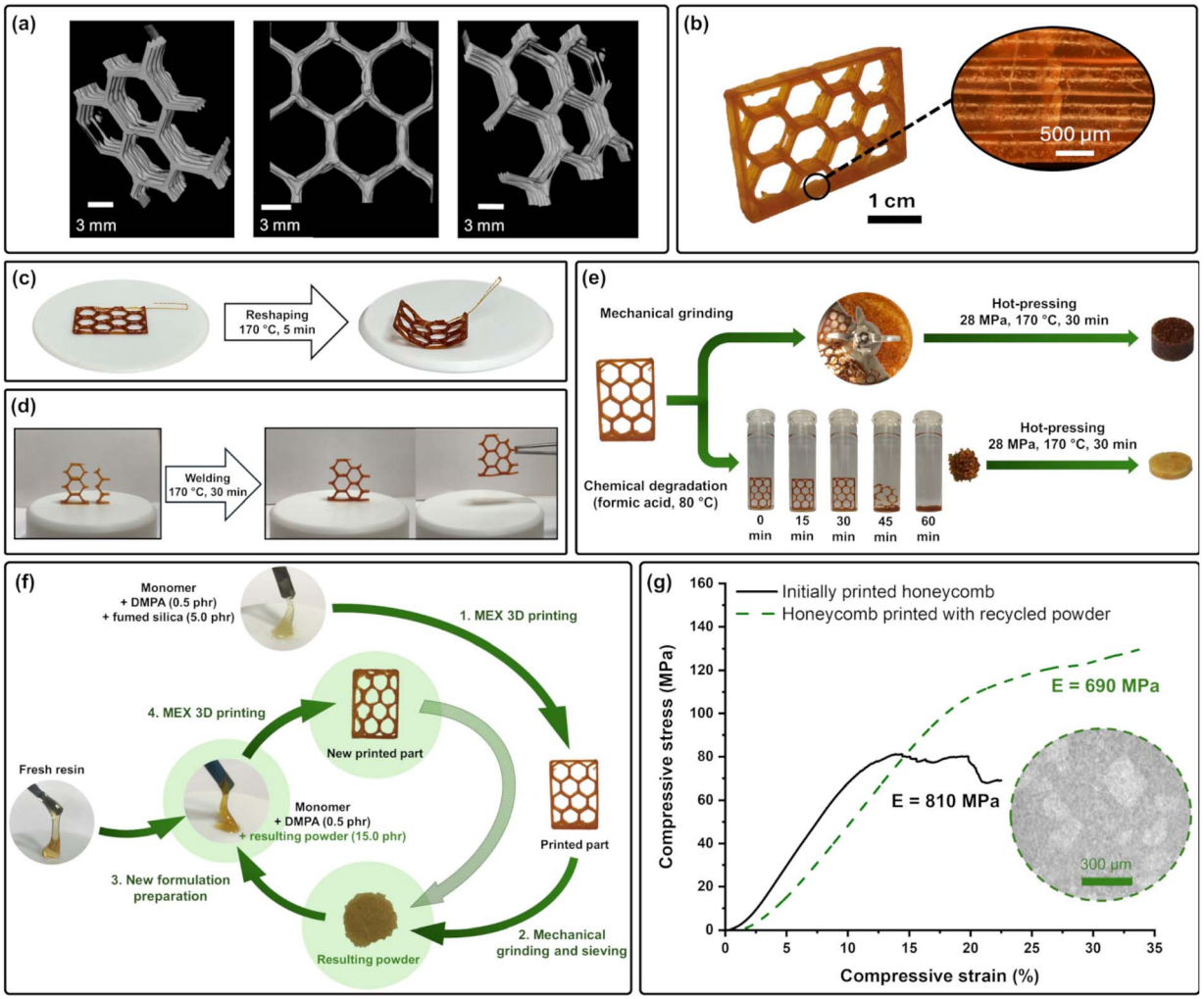

Fig. 7 (a) µCT images of a dual cured poly$_{UV+\Delta T}$(CHDM-PA-mea/mac$_2$) honeycomb; (b) microscopy of stacked layers of material in the poly$_{UV+\Delta T}$(CHDM-PA-mea/mac$_2$) honeycomb; (c) thermal reshaping of a poly$_{UV+\Delta T}$(CHDM-PA-mea/mac$_2$) honeycomb; (d) welding of the poly$_{UV+\Delta T}$(CHDM-PA-mea/mac$_2$) honeycomb (parts placed into an oven between two aluminium plates wrapped with Kapton® adhesive tape); (e) mechanical and chemical recycling of the poly$_{UV+\Delta T}$(CHDM-PA-mea/mac$_2$) honeycomb; (f) closed-loop recycling strategy using 3D printed parts for new additive manufacturing applications; (g) stress–strain profiles of poly$_{UV+\Delta T}$(CHDM-PA-mea/mac$_2$) honeycombs printed using silica and 3D printed part powder during compression tests with a µCT image of the printed bead containing the recycled powder.

the Nomex paper structure. In contrast, the material developed in this study achieves a compressive modulus of 810 MPa without such reinforcement. This performance, combined with its reprocessability and simplified fabrication, positions the material as a promising alternative for lightweight, recyclable structural applications.

4 Conclusions

This study is at the forefront of research on circular materials, integrating the benefits of additive manufacturing with bio-based and recyclable vitrimeric polybenzoxazines. These polymers are designed for recyclability by leveraging the introduction of dynamic bonds into their molecular structure. The result is a combination of attractive thermo-mechanical properties and vitrimeric behaviour that enables the material to be reshaped and recycled. Methacrylate functionalization expands the application of these materials to UV-assisted 3D printing, enabling UV curing and the creation of honeycomb structures as a printability demonstration. While excessive methacrylation reduces the amount of aliphatic –OH groups involved in transesterification, impacting vitrimeric properties, insufficient methacrylation hampers UV-assisted 3D printability. Our work identifies a good balance between these competing requirements, leading to the production of honeycomb structures that can be reshaped and recycled, with a T_α of 105 °C, 6% shrinkage, and a compressive modulus of 810 MPa. In addition, the reuse of printed material powder as a viscosity modifier for new printing tests has been successfully demonstrated, resulting in parts that retain their mechanical properties thanks to excellent filler–matrix interactions.

The manufacturing process developed in this work is much simpler than that of widely used alternatives, for instance, for Nomex honeycombs, which require several complex steps

including polymer processing, paper formation, resin impregnation, and curing—often at similar temperatures. In contrast, our monocomponent vitrimer can be shaped directly and reprocessed without additional formulation or treatment, offering a more energy-efficient and practical approach. Moreover, while the thermal post-treatment step requires a temperature of 170 °C, this condition must be considered in the context of the material entire life cycle. Unlike conventional thermosets, which typically require harsh, energy-intensive processes for end-of-life treatment with very low recycling efficiency, the vitrimer system presented here is reprocessable and reusable. This significantly reduces overall material waste and extends service life, aligning with sustainability goals.

Data availability

The data supporting this article have been included as part of the ESI.†

Author contributions

Charles Jehl: conceptualization, investigation, methodology, validation, writing – original draft – review & editing. Antoine Adjaoud: conceptualization, investigation, writing – review & editing. Ambre Meyer: investigation, validation. Vincent Boulic: investigation, writing – review & editing. Channya Hesse: investigation, writing – review & editing. Laura Puchot: methodology, writing – review & editing. Joamin Gonzalez-Gutierrez: data curation, investigation, validation, writing – review & editing. Alexander S. Shaplov: conceptualization, methodology, writing – review & editing. Daniel F. Schmidt: conceptualization, funding acquisition, methodology, writing – review & editing. Pierre Verge: conceptualization, methodology, supervision, writing – original draft – review & editing.

Conflicts of interest

There are no conflicts to declare.

Acknowledgements

This work was supported by the Luxembourg National Research Fund (FNR) through the Sustainable Polymer Composites - SusPoCo project (agreement number PRIDE21/16748260). The authors are also extremely thankful to Benoit Marcolini, Sebastien Gergen, Dr Reiner Dieden, and Dr Doriane Delfrari for their help in characterisation of the obtained polymer materials. The authors would also like to thank Tinatin Kouprava and Anaë Girault-Fodil for their helpful advice on the conceptual design of figures.

Notes and references

1 E. Morici and N. T. Dintcheva, *Polymers*, 2022, **14**, 4153.
2 K. L. Forsdyke and T. F. Starr, *Thermoset Resins Market Report*, iSmithers Rapra Publishing, 2002.
3 Md. G. Kibria, N. I. Masuk, R. Safayet, H. Q. Nguyen and M. Mourshed, *Int. J. Environ. Res.*, 2023, **17**, 20.
4 D. Montarnal, M. Capelot, F. Tournilhac and L. Leibler, *Science*, 2011, **334**, 965.
5 W. Denissen, J. M. Winne and F. E. Du Prez, *Chem. Sci.*, 2016, **7**, 30–38.
6 M. Guerre, C. Taplan, J. M. Winne and F. E. Du Prez, *Chem. Sci.*, 2020, **11**, 4855–4870.
7 W. Zou, J. Dong, Y. Luo, Q. Zhao and T. Xie, *Adv. Mater.*, 2017, **29**, 1606100.
8 M. Hayashi, *Polymers*, 2020, **12**, 1322.
9 A. Adjaoud, L. Puchot and P. Verge, *Polymer*, 2023, **287**, 126426.
10 A. Adjaoud, D. A. Boina, V. Boulic, C. Hesse, C. Jehl, C. Ziane, L. Puchot, A. S. Shaplov, D. F. Schmidt and P. Verge, in *Sustainable Green Chemistry in Polymer Research. Volume 2. Sustainable Polymers and Applications*, American Chemical Society, 2023, vol. 1451, pp. 49–84.
11 H. Ishida and D. J. Allen, *J. Polym. Sci., Part B: Polym. Phys.*, 1996, **34**, 1019.
12 H. Ishida and H. Y. Low, *Macromolecules*, 1997, **30**, 1099.
13 L. Bonnaud, B. Chollet, L. Dumas, A. A. M. Peru, A. L. Flourat, F. Allais and P. Dubois, *Macromol. Chem. Phys.*, 2019, **220**, 1800312.
14 D. Wang, B. Li, Y. Zhang and Z. Lu, *J. Appl. Polym. Sci.*, 2013, **127**, 516–522.
15 B. Lochab, I. K. Varma and J. Bijwe, *J. Therm. Anal. Calorim.*, 2010, **102**, 769.
16 K. Zhang, J. Liu, S. Ohashi, X. Liu, Z. Han and H. Ishida, *J. Polym. Sci., Part A: Polym. Chem.*, 2015, **53**, 1330.
17 H.-D. Kim and H. Ishida, *J. Phys. Chem. A*, 2002, **106**, 3271–3280.
18 S. B. Shen and H. Ishida, *Polym. Compos.*, 1996, **17**, 710.
19 H. Xiang, H. Ling, J. Wang, L. Song and Y. Gu, *Polym. Compos.*, 2005, **26**, 563–571.
20 C. Barile, C. Casavola and F. De Cillis, *Composites, Part B*, 2019, **162**, 122–128.
21 Y. Lyu and H. Ishida, *Prog. Polym. Sci.*, 2019, **99**, 101168.
22 L. Puchot, P. Verge, T. Fouquet, C. Vancaeyzeele, F. Vidal and Y. Habibi, *Green Chem.*, 2016, **18**, 3346.
23 N. K. Sini, J. Bijwe and I. K. Varma, *J. Polym. Sci., Part A: Polym. Chem.*, 2014, **52**, 7.
24 P. Thirukumaran, A. Shakila Parveen and M. Sarojadevi, *ACS Sustain. Chem. Eng.*, 2014, **2**, 2790.
25 L. Dumas, L. Bonnaud, M. Olivier, M. Poorteman and P. Dubois, *J. Mater. Chem. A*, 2015, **3**, 6012.
26 M. Monisha, N. Amarnath, S. Mukherjee and B. Lochab, *Macromol. Chem. Phys.*, 2019, **220**, 1800470.
27 M. Monisha, N. Yadav, S. B. Srivastava, S. P. Singh and B. Lochab, *J. Mater. Chem. A*, 2018, **6**, 2555–2567.
28 A. Adjaoud, B. Marcolini, R. Dieden, L. Puchot and P. Verge, *J. Am. Chem. Soc.*, 2024, **146**, 13367–13376.
29 A. Adjaoud, L. Puchot and P. Verge, *ACS Sustain. Chem. Eng.*, 2022, **10**, 594–602.
30 A. Adjaoud, A. Trejo-Machin, L. Puchot and P. Verge, *Polym. Chem.*, 2021, **12**, 3276.

31 A. Adjaoud, L. Puchot, C. E. Federico, R. Das and P. Verge, *Chem. Eng. J.*, 2023, **453**, 139895.
32 A. Trejo-Machin, L. Puchot and P. Verge, *Polym. Chem.*, 2020, **11**, 7026.
33 B. Akkus, B. Kiskan and Y. Yagci, *Polym. Chem.*, 2019, **10**, 5743–5750.
34 S. Sriharshitha, K. Krishnadevi and D. Prasanna, *RSC Adv.*, 2022, **12**, 26934–26944.
35 X. Wang, S. Zhang, Y. He, W. Guo and Z. Lu, *Polymers*, 2022, **14**, 2234.
36 Z. Qiao, M. Wang, J. Jiang, H. Liu, M. Wang, W. Zhao and Z. Wang, *ACS Sustain. Chem. Eng.*, 2022, **10**, 9113–9122.
37 X.-L. Sha, L. Yuan, G. Liang and A. Gu, *Polymer*, 2020, **202**, 122673.
38 S. Gao, Y. Liu, S. Feng and Z. Lu, *J. Mater. Chem. A*, 2019, **7**, 17498.
39 P. Wang, S. Zhang, W. Xu, T. Xiao and Q. Ran, *ACS Sustain. Chem. Eng.*, 2021, **9**, 7913–7921.
40 S. Ford and M. Despeisse, *J. Clean. Prod.*, 2016, **137**, 1573–1587.
41 T. D. Ngo, A. Kashani, G. Imbalzano, K. T. Q. Nguyen and D. Hui, *Composites, Part B*, 2018, **143**, 172–196.
42 A. H. Alami, A. Ghani Olabi, A. Alashkar, S. Alasad, H. Aljaghoub, H. Rezk and M. A. Abdelkareem, *Ain Shams Eng. J.*, 2023, **14**, 102516.
43 M. H. Mobarak, Md. A. Islam, N. Hossain, Md. Z. Al Mahmud, Md. T. Rayhan, N. J. Nishi and M. A. Chowdhury, *Appl. Surf. Sci. Adv.*, 2023, **18**, 100462.
44 J. Hoerber, J. Glasschroeder, M. Pfeffer, J. Schilp, M. Zaeh and J. Franke, *Proced. CIRP*, 2014, **17**, 806–811.
45 A. D. Nugraha, M. Syahril and M. A. Muflikhun, *Heliyon*, 2023, **9**, e14706.
46 F. Craveiro, J. P. Duarte, H. Bartolo and P. J. Bartolo, *Autom. Constr.*, 2019, **103**, 251–267.
47 A. Vyatskikh, A. Kudo, S. Delalande and J. R. Greer, *Mater. Today Commun.*, 2018, **15**, 288–293.
48 A. Oleff, B. Küster, M. Stonis and L. Overmeyer, *Prog. Addit. Manuf.*, 2021, **6**, 705–730.
49 M. a. S. R. Saadi, A. Maguire, N. T. Pottackal, M. S. H. Thakur, M. Md. Ikram, A. J. Hart, P. M. Ajayan and M. M. Rahman, *Adv. Mater.*, 2022, **34**, 2108855.
50 B. Krishna Kumar and T. J. Dickens, *J. Appl. Polym. Sci.*, 2023, **140**, e53304.
51 X. Wan, L. Luo, Y. Liu and J. Leng, *Adv. Sci.*, 2020, **7**, 2001000.
52 Y. Lu, K. W. J. Ng, H. Chen, X. Chen, S. K. J. Lim, W. Yan and X. Hu, *Chem. Commun.*, 2021, **57**, 3375–3378.
53 Y. Yang, X. Xu, Z. Li, X. Yao, D. Kang, Y. Lu, Y. Wang, Y. Guo and X. Wang, *Mater. Lett.*, 2023, **345**, 134448.
54 J. J. Weigand, C. I. Miller, A. P. Janisse, O. D. McNair, K. Kim and J. S. Wiggins, *Polymer*, 2020, **189**, 122193.
55 N. D. Arun, H. Yang, L. Yao and A. W. Feinberg, *Adv. Mater. Technol.*, 2023, **8**, 2201542.
56 L. Jin, T. Agag, Y. Yagci and H. Ishida, *Macromolecules*, 2011, **44**, 767–772.
57 A. Trejo-Machin, P. Verge, L. Puchot and R. Quintana, *Green Chem.*, 2017, **19**, 5065–5073.
58 C. Berti, E. Binassi, M. Colonna, M. Fiorini, G. Kannan, S. Karanam, M. Mazzacurati, I. Odeh and M. Vannini, *ChemSusChem*, 2016, **9**, 3102–3112.
59 X. Guo, J. Xin, X. Lu, B. Ren and S. Zhang, *RSC Adv.*, 2014, **5**, 485–492.
60 B. Kiskan, B. Koz and Y. Yagci, *J. Polym. Sci., Part A:Polym. Chem.*, 2009, **47**, 6955–6961.
61 R. Kudoh, A. Sudo and T. Endo, *Macromolecules*, 2010, **43**, 1185–1187.
62 B. Lochab, M. Monisha, N. Amarnath, P. Sharma, S. Mukherjee and H. Ishida, *Polymers*, 2021, **13**, 1260.
63 F. I. Altuna, C. E. Hoppe and R. J. J. Williams, *Eur. Polym. J.*, 2019, **113**, 297.
64 J. Han, T. Liu, C. Hao, S. Zhang, B. Guo and J. Zhang, *Macromolecules*, 2018, **51**, 6789–6799.
65 Y. Cui, J. Yang, D. Lei and J. Su, *Ind. Eng. Chem. Res.*, 2020, **59**, 11381–11388.
66 C. Wang, S. Ma, D. Li, J. Zhao, H. Zhou, D. Wang, D. Zhou, T. Gan, D. Wang, C. Liu, C. Qu and C. Chen, *ACS Appl. Mater. Interfaces*, 2021, **13**, 15690–15700.
67 Z. C. Eckel, C. Zhou, J. H. Martin, A. J. Jacobsen, W. B. Carter and T. A. Schaedler, *Science*, 2016, **351**, 58–62.
68 Z. Wen and M. Li, *Materials*, 2021, **14**, 4410.
69 S. Antony, A. Cherouat and G. Montay, *Appl. Compos. Mater.*, 2020, **27**, 935–953.
70 P. Dittanet and R. A. Pearson, *Polymer*, 2012, **53**, 1890–1905.